Propagation Dynamics of Airy Water-Wave Pulses

Shenhe Fu,[1,2] Yuval Tsur,[1] Jianying Zhou,[2] Lev Shemer,[3] and Ady Arie[1,*]
[1]Department of Physical Electronics, Faculty of Engineering, Tel-Aviv University, Tel-Aviv 69978, Israel
[2]State Key Laboratory of Optoelectronic Materials and Technologies, Sun Yat-sen University, Guangzhou 510275, China
[3]School of Mechanical Engineering, Faculty of Engineering, Tel-Aviv University, Tel-Aviv 69978, Israel
(Received 29 January 2015; published 13 July 2015)

We observe the propagation dynamics of surface gravity water waves, having an Airy function envelope, in both the linear and the nonlinear regimes. In the linear regime, the shape of the envelope is preserved while propagating in an 18-m water tank, despite the inherent dispersion of the wave packet. The Airy wave function can propagate at a velocity that is slower (or faster if the Airy envelope is inverted) than the group velocity. Furthermore, the introduction of the Airy wave packet as surface water waves enables the observation of its position-dependent chirp and cubic-phase offset, predicted more than 35 years ago, for the first time. When increasing the envelope of the input Airy pulse, nonlinear effects become dominant, and are manifested by the generation of water-wave solitons.

DOI: 10.1103/PhysRevLett.115.034501 PACS numbers: 47.35.Bb, 05.45.Yv, 47.35.Fg

In 1979, in the framework of quantum mechanics, the Airy wave packet was shown to be a solution of the Schrödinger equation for a free particle [1]. This wave packet exhibits peculiar features—acceleration without any external force, and shape preservation in a dispersive medium. In 2007, Christodoulides *et al.* implemented these concepts in optics, by showing that an ideal Airy optical beam follows a bent parabolic trajectory in free space and remains diffraction free [2]. Research on Airy beams has become very intense in recent years, and many potential applications involving Airy beams have already been demonstrated, including optical manipulation of microparticles [3], generation of curved plasma channels [4], light induced optical routing [5], and superresolution fluorescence imaging [6]. Airy light pulses have also been demonstrated in the time domain, and have been used to form light bullets [7,8], which overcome both diffraction and dispersion during propagation. Apart from these studies on the linear case, the nonlinear optical generation [9] and the evolution of Airy beams in various nonlinear quadratic [10,11], cubic [11], and photorefractive [12] media have been studied. Solitons off-shooting from Airy pulses [13] and Airy beams [14] in strong Kerr focusing nonlinearity have been theoretically predicted, but have not been observed experimentally up till now.

The concept of self-accelerating Airy beams has been extended beyond light waves, leading to the prediction [15] and the subsequent realization of Airy surface plasmon polariton beams [16–18], as well as the experimental generation of electron Airy beams [19].

It is interesting to note that all measurements of Airy waves have so far concentrated on the shape of the wave's envelope, while disregarding the phase, possibly owing to the difficulty in directly measuring the carrier phase of these high frequency wave packets [20]. The phase dependence of the Airy wave function was already theoretically predicted in the original paper [1] more than 35 years ago. It includes a phase term that is a product of the propagation and temporal coordinates, and an offset term that is proportional to the third power of the propagation coordinate. This phase dependence had not been observed experimentally so far.

Wave propagation dynamics in optics in many aspects is analogous to that of water gravity waves; both phenomena share similar physics, as discussed in relation to the appearance of so-called "rogue" waves [21]. In this Letter, we take advantage of the analogy between optics and water-wave theory to investigate the Airy pulse propagation in a wave tank for the first time (underwater Airy beams were recently realized [22]). This allows us to study the previously inaccessible properties of the Airy pulse, both in the linear and the nonlinear regimes.

Zakharov [23] derived a general equation describing the temporal evolution of deep-water gravity waves in Fourier space at the 3rd order in the characteristic wave steepness $\varepsilon = k_0 a_0$, where k_0 and a_0 are the characteristic wave number and amplitude. In the same paper, invoking the narrow spectrum approximation, the so-called nonlinear Schrödinger equation was derived for the complex wave envelope $a(x,t)$. Dysthe [24] suggested a 4th order modification of the nonlinear Schrödinger equation by relaxing the requirement of vanishing spectral width. Following Refs. [25–27], the spatial version of the Dysthe equation in normalized form is given by

$$\begin{aligned}\frac{\partial A}{\partial \xi} + i\frac{\partial^2 A}{\partial \tau^2} + i\frac{1}{\gamma^2}|A|^2 A + 8\frac{\varepsilon}{\gamma}|A|^2\frac{\partial A}{\partial \tau} \\ + 2\frac{\varepsilon}{\gamma}A^2\frac{\partial A^*}{\partial \tau} + 4i\frac{\varepsilon}{\gamma}A\frac{\partial \Phi}{\partial \tau}\Big|_{Z=0} = 0, \\ 4\frac{\partial^2 \Phi}{\partial \tau^2} + \frac{\partial^2 \Phi}{\partial Z^2} = 0, \qquad (Z<0). \end{aligned} \tag{1}$$

The scaled dimensionless variables are related to physical units according to $\xi = (\gamma\varepsilon)^2 k_0 x$, $\tau = \gamma\varepsilon\omega_0(x/c_g - t)$, $A = a/a_0$, $\Phi = \phi/(\omega_0 a_0^2)$, and $Z = \gamma\varepsilon k_0 z$. Here, x and z denote the propagation and vertical coordinates, respectively, $z = 0$ at the free surface, t is the real time, and γ is a scale factor, introduced to assure conformity between the optical and the hydrodynamic formulations. The wave number $k_0 = 2\pi/\lambda_0$, where λ_0 is the carrier wavelength. The angular frequency ω_0 satisfies the deep water dispersion relation $\omega_0^2 = k_0 g$, where g is the acceleration due to gravity. The water-wave group velocity $c_g = d\omega/dk = \omega_0/2k_0$. A is the normalized group envelope. The water velocity potential ϕ satisfies $\partial\Phi/\partial Z = \partial|A|^2/\partial\tau$ (for $Z = 0$), and $\partial\Phi/\partial Z = 0$ (for $Z = -\infty$).

In this work, we study first the propagation dynamics of low amplitude Airy water-wave pulses, described by the linearized governing equation. Higher amplitude nonlinear pulses are considered at a later stage.

Retaining linear terms only in Eq. (1) yields [27]

$$\frac{\partial A}{\partial \xi} + i\frac{\partial^2 A}{\partial \tau^2} = 0. \tag{2}$$

As is known, Eq. (2) admits an ideal solution with the Airy form [1,2]: $A(\xi,\tau) = \mathrm{Ai}(\tau - \xi^2)\exp[-i\tau\xi + (2i/3)\xi^3]$. Here, Ai stands for the Airy function. At $\xi = 0$, $A(\xi = 0,\tau) = \mathrm{Ai}(\tau) = \mathrm{Ai}(-t/t_s)$, where t_s determines the size of the Airy main lobe and, hence, the acceleration. Comparison of the definition of τ in optics and water-wave theory leads to the relation $t_s = 1/(\gamma\varepsilon\omega_0)$. It is seen from the solution that the pulse $A(\xi,\tau)$ preserves its Airy shape while propagating along ξ and follows a parabolic trajectory described by

$$t(x) = x/c_g + \nu k_0^2 x^2/(\omega_0^4 t_s^3), \tag{3}$$

where $\nu = \pm 1$. At $\nu = 1$ (-1), $t(x)$ describes the trajectory of the Airy pulse (time-inverted Airy pulse). Ideal Airy water-wave pulses carry an infinite amount of energy, whereas in practice these pulses should be truncated by an exponential or a Gaussian window [2]. Here, exponential truncation is used; thus, the initial condition is written as $A(x = 0, t) = \mathrm{Ai}(t/t_s)\exp(\alpha t/t_s)$, where α is positive. Truncated Airy pulses evolve according to [2]

$$A(\xi,\tau) = \mathrm{Ai}(\tau - \xi^2 - i2\alpha\xi) \times \exp(\alpha\tau - 2\alpha\xi^2 - i\tau\xi - i\alpha^2\xi + i\tfrac{2}{3}\xi^3). \tag{4}$$

The experiments were performed in an 18 m long, 1.2 m wide, and $h = 0.6$ m deep laboratory wave tank. Waves are excited by a computer controlled paddle-type wave maker placed at one end of the water tank. A wave energy absorbing beach is placed at the other end. To eliminate the effect of the beach, measurements were limited to distances not exceeding 14 m from the wave maker. The instantaneous water surface elevation at any fixed location along the tank is measured by four wave gauges mounted on a bar that is parallel to the tank side walls. The bar with the gauges is fixed to an instrument carriage that can be shifted along the tank and is controlled by the computer. The temporal surface elevation of the Airy pulse at the wave maker has the following form:

$$\eta(t, x = 0) = a_0 A(t)\cos(\omega_0 t), \tag{5}$$

where the maximum value of $A(t)$ at $x = 0$ is normalized to unity so that a_0 is the maximum amplitude of the envelope. In the experiment $\lambda_0 = 0.76$ m, so that the dimensionless depth $k_0 h = 4.96 > \pi$, satisfying the deep water condition [28]; the corresponding group velocity is $c_g = 0.54$ m/s. As discussed in Ref. [28], for the selected carrier wavelength the dissipation is weak and can be neglected.

According to Eq. (4), in the linear approximation, the Airy pulse should preserve its shape while propagating along the wave tank. We confirm this assertion with the measurements shown in Fig. 1, illustrating the evolution dynamics of the Airy pulses. Both the experimental and theoretical results indicate that the Airy shape is preserved well during evolution along the tank.

The features of Airy pulses such as nonspreading and self-acceleration are more difficult to observe with large t_s in our tank due to its limited length; hence, to demonstrate those properties smaller values were selected. Figure 2 demonstrates the weakly spreading feature of the Airy pulses during propagation in the water tank, with $t_s = 1.2$ s. To illustrate the property, a comparison between spreading of Airy and Gaussian pulses was made. As expected, the Airy pulse envelopes remain almost nonspreading, as shown in Figs. 2(a)–2(c) experimentally and theoretically. Furthermore, the square root of second-order moment for the Airy main lobe was measured using [29]

$$\sigma^2 = \frac{4\int_{-\infty}^{\infty}(t - \bar{t})^2|\eta|^2 dt}{\int_{-\infty}^{\infty}|\eta|^2 dt}, \qquad \bar{t} = \frac{\int_{-\infty}^{\infty} t|\eta|^2 dt}{\int_{-\infty}^{\infty}|\eta|^2 dt} \tag{6}$$

(the integral is performed over the main lobe) and is shown in Fig. 2(f), thereby confirming the weakly spreading feature of Airy wave pulses. The Gaussian pulse envelope having the same width as that of the main lobe of the Airy

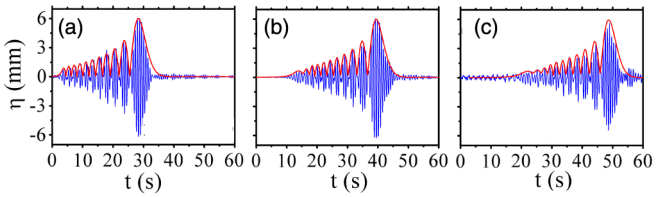

FIG. 1 (color online). Experimental elevations (blue curves) and theoretical envelopes (red curves) of Airy wave packets measured at (a) $x = 1.43$ m, (b) 7.46 m, and (c) 12.50 m, for $a_0 = 6.0$ mm ($\varepsilon = 0.05$), $\alpha = 0.1$, and $t_s = 2.0$ s.

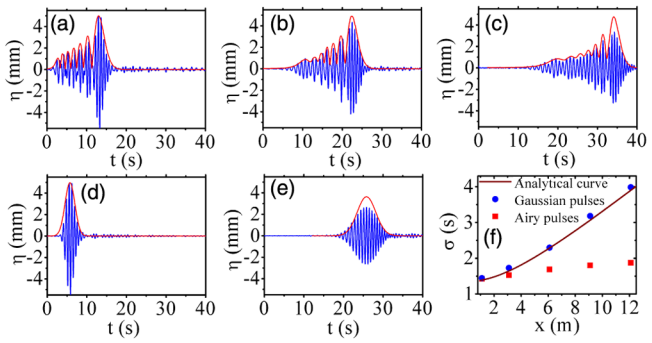

FIG. 2 (color online). (a)–(c) Experimental elevations (blue curves) and theoretical envelopes (red curves) of Airy wave packets at (a) $x = 1.10$ m, (b) 6.10 m, and (c) 12.10 m, for $a_0 = 5.0$ mm ($\varepsilon = 0.04$), $\alpha = 0.1$, and $t_s = 1.2$ s. (d),(e) Gaussian pulse measured at (d) $x = 1.10$ m and (e) 12.10 m. (f) The measurements of the second-order moment for Airy and Gaussian wave pulses. The solid brown line is the analytical result for the Gaussian pulse.

pulse exhibits significant broadening, see Figs. 2(d) and 2(e). The pulse width broadens to more than twice its original width at $x = 12.10$ m. The measured σ of the Gaussian pulse agrees well with the theoretical result: $\sigma = \sqrt{1 + (x/x_0)^2}\sigma_0$, where σ_0 is the initial square root of the second-order moment and $x_0 = g\sigma_0^2/4$ is the dispersion length, see Fig. 2(f). A slight difference between experiment and theory in Figs. 2(c) and 2(e), as well as the weak spreading of Airy pulses in Fig. 2(f), is explained by partial experimental fulfillment of the slowly varying envelope approximation. A short pulse width in the experiment would lead to deviation from the theory due to the low carrier frequency. Note that a small number of side lobes that can be used to compensate the dispersion of the main lobe [30] further contributes to the discrepancy.

A noteworthy feature of Airy wave packets is their so-called "self-acceleration." In the experiment, the temporal accelerations of the local envelope maxima of the Airy and time-inverted Airy water-wave pulses were investigated, with $t_s = 0.7$ s, keeping other parameters unaffected. From the results shown in Fig. 3, it can be deduced that for different fixed locations, the larger x gives rise to a larger temporal shift between the main lobes of the Airy and the time-inverted Airy pulses, which implies the different propagating group velocities of these two kinds of Airy wave packets, i.e., self-accelerating during propagation. This phenomenon is clearly demonstrated in Fig. 4, illustrating the distinct parabolic trajectories of the main lobes of the Airy (red curves) and time-inverted Airy pulses (brown curves), as compared with the linear trajectory of the Gaussian pulses (blue curves). As the maxima of these pulse envelopes were located at different time points at the origin, these curves shown in Fig. 4 were shifted to the same zero time point at $x = 0$ so that the trajectories can be well described by the analytical expressions, see Eq. (3),

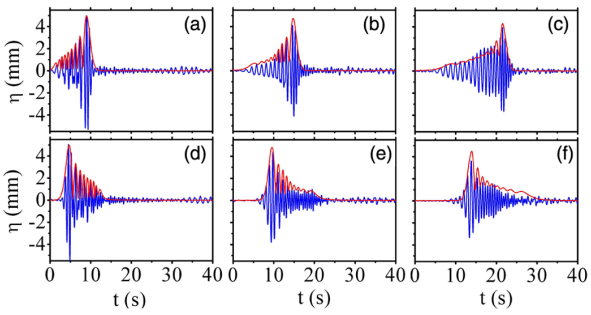

FIG. 3 (color online). Evolutions of Airy (a)–(c) and inverted Airy (d)–(f) wave packets with $t_s = 0.7$ s: experimental elevations (blue curves) and theoretical envelopes (red curves) at (a), (d) $x = 1.00$ m, (b),(e) $x = 4.00$ m, and (c),(f) $x = 7.00$ m.

with $\nu = 1$ for the Airy pulses, $\nu = -1$ for the time-inverted Airy pulses, and $\nu = 0$ for the Gaussian pulses. The solid lines in Fig. 4 are the analytical results, showing good agreement with the experiments. Self-healing of the Airy wave packets was also demonstrated experimentally and numerically, see the Supplemental Material [31].

We present the first direct experimental measurements of the phase of Airy wave packets during propagation. Based on Eq. (4), the phase for the Airy wave packets can be expressed as $\psi(\xi, \tau) = \varphi_{\mathrm{Ai}} + \varphi$, where φ_{Ai} is the phase of the Airy function and $\varphi = -\tau\xi - \alpha^2\xi + 2/3\xi^3$ is the induced evolution phase of the envelope during propagation. For the truncated Airy pulses, φ_{Ai} can be obtained numerically. In our experiment, the phase of the Airy water-wave envelope is modulated by a carrier wave: $\eta(x, t) = \mathrm{Re}[a_0 A(x, t) \exp(ik_0 x - i\omega_0 t)]$ [32]. Thus the phase of the elevation wave groups in the experiments is described by $\psi = \varphi_{\mathrm{Ai}} + \varphi + k_0 x - \omega_0 t$.

To demodulate the phase φ from the carrier wave, we extract the local maximum and minimum values of the elevation wave groups, marked in red and green dots respectively at different times t_j (j is the index of these points), see Figs. 5(a), 5(c), and 5(e). At these marked

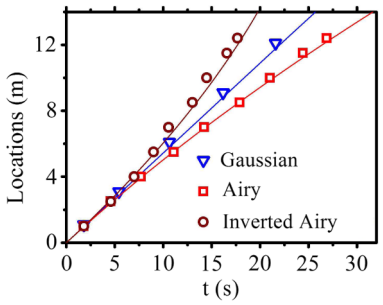

FIG. 4 (color online). The parabolic trajectories of the Airy (red curves) and inverted Airy (brown curves) wave packets, using the same parameters as in Fig. 3. The blue curve corresponds to the linear trajectory of a Gaussian pulse, as shown in Fig. 2. The solid lines are analytical results, according to Eq. (3); the symbols are measurements.

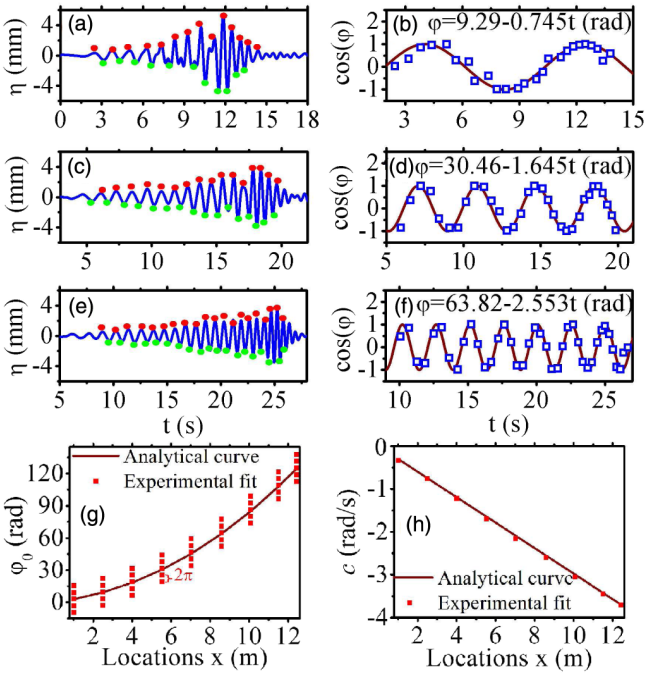

FIG. 5 (color online). (a),(c),(e) are the measured elevation Airy wave groups with the parameters of Fig. 3, while (b),(d),(f) are the corresponding phase variations with time, at (a),(b) $x = 2.50$ m, (c),(d) 5.53 m, and (e),(f) 8.58 m. The expressions in (b),(d),(f) describe the analytical phases. (g) The phase offset φ_0 as a cubic function of x, and (h) the slope c of the linear time-dependent function of the phase.

points, we have the relation $\cos(\psi_j) = \pm 1$ [for red (green) points, it equals 1 (-1)]. Therefore, the induced phase φ at a fixed location can be expressed as $\varphi_j = \arccos(\pm 1) + \omega_0 t_j - \varphi_{\mathrm{Ai},j} - k_0 x$. As an example, given the elevation wave groups measured at $x = 2.50$ m, see Fig. 5(a), the corresponding phase variation with time in the form of a cosine function is depicted in Fig. 5(b). The blue scattered dots show the experimental outcome while the solid brown line is the theoretical result according to the analytical expression shown in Fig. 5(b). Using the same method, for the measurements at $x = 5.53$ and 8.58 m, see Figs. 5(c) and 5(e), the phases φ of the Airy envelopes can be determined too, as displayed in Figs. 5(d) and 5(f). As expected, at a fixed location, the induced phase φ is a linear function of time t, see Eq. (4). The slope of the linear function of the phase is determined by t_s and the location x. In the experiment, the phase at specific locations is also supposed to be expressed as $\varphi = \varphi_0 + ct$, where φ_0 is the initial phase shift and c is the slope of the function. The value of c can be obtained directly at different locations by fitting the experimental results, as shown in Fig. 5(h). As for the phase offset φ_0, owing to the phase ambiguity of the inverse cosine function, a set of possible phases at each location is obtained, having a 2π spacing between them. Fortunately, one of these points coincides with the theoretical cubic position-dependence phase shift, see Fig. 5(g), thereby enabling us to remove the phase ambiguity. Both the experimental and theoretical results show that for larger values of x, the value of the slope c is also increasing linearly, which leads to a rapid oscillation of the phase, seen from Figs. 5(b), 5(d), and 5(f). These measurements therefore explicitly confirm the linear dependence of the Airy wave phase, and indirectly indicate the cubic dependence of the phase offset.

Finally, we investigated the effect of nonlinearity on the propagation dynamics of the Airy water-wave pulses. Observations of the transition of Airy pulses from stability to instability owing to the Kerr-type nonlinearity are presented here for the first time. For a sufficiently low incident amplitude, i.e., $a_0 = 5$ mm, where the nonlinearity is negligible, the Airy pulse wave packets self-accelerated along a parabolic trajectory during the propagation, see Figs. 6(a) and 6(b). The Airy pulse preserves its shape within nearly 4 m, and begins to broaden due to dispersion (note that here the pulse width is nearly half that of Fig. 2; hence, the broadening is more pronounced). When the amplitude was increased to $a_0 = 17$ mm, it was observed that the Airy pulses stabilized (the so-called self-accelerating self-trapped Airy pulse [11]): not only did they self-accelerate along the parabolic trajectory, but the dispersion was compensated by the induced weak nonlinearity. This leads to preservation of the shape over the longer distance of nearly 8 m, approximately twice as long as the linear case, see Figs. 6(c) and 6(d). For an even higher amplitude $a = 23$ mm, strong Kerr nonlinearity was induced, as evident from widening of the corresponding spectra [31]. In this case, the central lobe of the Airy pulse started compressing during propagation, further increasing its

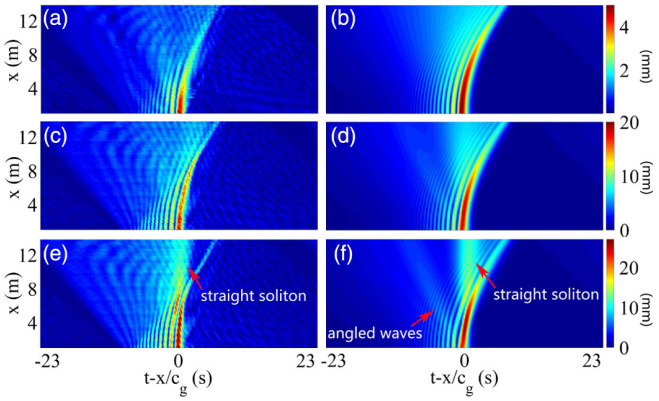

FIG. 6 (color online). Evolutions of Airy envelopes [left, obtained from the measurements by the Hilbert transform; right. simulated based on Eq. (1)] with $t_s = 0.65$ s and $\alpha = 0.1$, in a frame of reference moving at speed c_g. Measurements were performed at (a),(b) $a_0 = 5$ mm, $\varepsilon = 0.04$, (c),(d) $a_0 = 17$ mm, $\varepsilon = 0.14$, and (e),(f) $a_0 = 23$ mm, $\varepsilon = 0.19$. The color bar units are millimeters. For the $a_0 = 23$ mm evolution movie see Ref. [31].

amplitude, which eventually leads to a collapse and an emission of a stationary soliton, shown in Figs. 6(e) and 6(f) and in the nonlinear evolution movie in Ref. [31]. The numerical simulations were carried out using the nonlinear Eq. (1). Both experiments and simulations show a negligible effect of the soliton emission on the original parabolic trajectory. The numerical simulation shows that there are also additional small-amplitude waves emitted from the weaker side lobes at an angle to the straight soliton, see Fig. 6(f). These waves are similar to the solitons predicted in Ref. [11]. However, these are not observed clearly in the experiment, possibly owing to their low amplitude.

In conclusion, we presented the first observation for the propagation dynamics of Airy water-wave pulses in both the linear and the nonlinear regimes. In the linear regime, we discussed the nonspreading, self-accelerating, and self-healing [31] properties of Airy pulses. It is worth mentioning that the evolution phase of Airy wave packets predicted more than 35 years ago [1] has been confirmed experimentally in our Letter for the first time. It should be emphasized that a direct phase measurement of Airy wave packets is inaccessible in optical experiments [2]. where owing to the high carrier frequency only the signal intensity can be measured and therefore the information of the phase is lost. We further note that our measurement technique is not limited to Airy wave packets, and it provides us with an opportunity to fully study the dynamics of the envelope and phase of other kinds of water-wave packets. In the nonlinear regime, we observed the transition of Airy pulses in water waves from stability to instability with Kerr-type nonlinearity. Previous predictions of the self-accelerating self-trapped Airy pulse [11], as well as soliton shedding [13,14] from Airy pulses, were observed experimentally. We believe that the results presented here are new and of interest both in optics and hydrodynamics, as analogies between these two fields have yielded interesting outcomes [21].

This work was supported by DIP, the German-Israeli Project Cooperation, National Basic Research Program (Grant No. 2012CB921904), the U.S.-Israel Binational Science Foundation (Grant No. 2010219), and the Overseas Study Program of the China Scholarship Council. We thank A. Zavadsky and B. K. W. Ee for technical assistance.

*ady@eng.tau.ac.il

[1] M. V. Berry and N. L. Balazs, Am. J. Phys. **47**, 264 (1979).
[2] G. A. Siviloglou, J. Broky, A. Dogariu, and D. N. Christodoulides, Phys. Rev. Lett. **99**, 213901 (2007).
[3] J. Baumgartl, M. Mazilu, and K. Dholakia, Nat. Photonics **2**, 675 (2008).
[4] P. Polynkin, M. Kolesik, J. V. Moloney, G. A. Siviloglou, and D. N. Christodoulides, Science **324**, 229 (2009).
[5] P. Rose, F. Diebel, M. Boguslawski, and C. Denz, Appl. Phys. Lett. **102**, 101101 (2013).
[6] S. Jia, J. C. Vaughan, and X. Zhuang, Nat. Photonics **8**, 302 (2014).
[7] A. Chong, W. H. Renninger, D. N. Christodoulides, and F. W. Wise, Nat. Photonics **4**, 103 (2010).
[8] D. Abdollahpour, S. Suntsov, D. G. Papazoglou, and S. Tzortzakis, Phys. Rev. Lett. **105**, 253901 (2010).
[9] T. Ellenbogen, N. V. Bloch, A. G. Padowicz, and A. Arie, Nat. Photonics **3**, 395 (2009).
[10] I. Dolev, I. Kaminer, A. Shapira, M. Segev, and A. Arie, Phys. Rev. Lett. **108**, 113903 (2012).
[11] I. Kaminer, M. Segev, and D. N. Christodoulides, Phys. Rev. Lett. **106**, 213903 (2011).
[12] S. Jia, J. Lee, J. W. Fleischer, G. A. Siviloglou, and D. N. Christodoulides, Phys. Rev. Lett. **104**, 253904 (2010).
[13] Y. Fattal, A. Rudnick, and D. M. Marom, Opt. Express **19**, 17298 (2011).
[14] I. M. Allayarov and E. N. Tsoy, Phys. Rev. A **90**, 023852 (2014).
[15] A. Salandrino and D. N. Christodoulides, Opt. Lett. **35**, 2082 (2010).
[16] A. Minovich, A. E. Klein, N. Janunts, T. Pertsch, D. N. Neshev, and Y. S. Kivshar, Phys. Rev. Lett. **107**, 116802 (2011).
[17] P. Zhang, S. Wang, Y. Liu, X. Yin, C. Lu, Z. Chen, and X. Zhang, Opt. Lett. **36**, 3191 (2011).
[18] L. Li, T. Li, S. M. Wang, C. Zhang, and S. N. Zhu, Phys. Rev. Lett. **107**, 126804 (2011).
[19] N. V. Bloch, Y. Lereah, Y. Lilach, A. Gover, and A. Arie, Nature (London) **494**, 331 (2013).
[20] Methods for measuring the carrier-envelope phase of ultrashort optical pulses were available and were used for applications such as absolute frequency measurements and high harmonic generation, see H. R. Telle, G. Steinmeyer, A. E. Dunlop, J. Stenger, D. H. Sutter, and U. Keller, Appl. Phys. B **69**, 327 (1999).
[21] J. M. Dudley, F. Dias, M. Erkintalo, and G. Genty, Nat. Photonics **8**, 755 (2014).
[22] U. Bar-Ziv and M. Segev (in press).
[23] V. E. Zakharov, J. Appl. Mech. Tech. Phys. **9**, 190 (1968).
[24] K. B. Dysthe, Proc. R. Soc. A **369**, 105 (1979).
[25] E. Lo and C. C. Mei, J. Fluid Mech. **150**, 395 (1985).
[26] E. Kit and L. Shemer, J. Fluid Mech. **450**, 201 (2002).
[27] L. Shemer and B. Dorfman, Nonlinear Proc. Geophys. **15**, 931 (2008).
[28] L. Shemer, K. Goulitski, and E. Kit, Eur. J. Mech. B, Fluids **26**, 193 (2007).
[29] H. Weber, Opt. Quantum Electron. **24**, S1027 (1992).
[30] R. Schley, I. Kaminer, E. Greenfield, R. Bekenstein, Y. Lumer, and M. Segev, Nat. Commun. **5**, 5189 (2014).
[31] See Supplemental Material at http://link.aps.org/supplemental/10.1103/PhysRevLett.115.034501 for (a) the self-healing property of the pulse, (b) the Airy pulse frequency spectra, and (c) the $a_0 = 23$ mm nonlinear evolution movie.
[32] L. Shemer and L. Alperovich, Phys. Fluids **25**, 051701 (2013).